Numerical simulations of atomic-scale disordering processes at impact between two rough crystalline surfaces

F. Delogu[1,*] and G. Cocco[2]
[1]*Dipartimento di Ingegneria Chimica e Materiali, Università di Cagliari, piazza d'Armi, I-09123 Cagliari, Italy*
[2]*Dipartimento di Chimica, Università di Sassari, via Vienna 2, I-07100 Sassari, Italy*
(Received 22 December 2005; revised manuscript received 25 May 2006; published 7 July 2006)

Numerical calculations have been used to throw light on the mechanical deformation and the atomic mixing processes taking place when two different metallic systems collide at low temperature. To this end, two semicrystals terminating with a free surface were pushed each against the other at a given relative velocity. Surfaces of different roughness were considered under different impact conditions. Simple mechanical loads on plane surfaces did not induce any significant mixing of atomic species at the interface, observed instead in collisions involving either rough surfaces or plane surfaces undergoing a relative sliding. In the case of rough surfaces, the local contact between the semicrystals is initially sustained by surface asperities. The atoms there located experience thus sudden mechanical loads and an unusual localization of kinetic energy, which enhance their mobility and favor the mixing process. A diffuse interfacial region with a disordered structure correspondingly appears. Its structural features were not significantly modified by the thermal relaxation processes occurring after the compressive load removal.

DOI: 10.1103/PhysRevB.74.035406 PACS number(s): 68.35.Af, 68.35.Ct, 61.43.Dq

I. INTRODUCTION

The plastic deformation of a crystalline solid takes place via the formation and interaction of point, line, and plane defects.[1–3] The accumulation of local atomic strains results in the storage of excess potential energy and the consequent enhancement of the chemical reactivity,[1–3] the occurrence of phase transformations being correspondingly favored.[4–6] Such behavior underlies the mechanochemistry as well as the modern techniques of powder metallurgy,[4–6] which generally rely upon the repeated mechanical loading of powder particles trapped between colliding surfaces and the related occurrence of local shear events on the microscopic scale.[6–8]

The localization of considerable amounts of energy in relatively small volumes of solid phase determines the accumulation of strain and the nucleation of defects.[9–20] Fast local processes of mass transport and mixing occur assisted by complex aggregates of atoms with defective coordination.[17,19,20] These relax and to a large extent disappear as a consequence of thermal equilibration processes when the shear stresses are removed.[19,20]

Despite the deeper insight provided by these mechanistic scenarios[9–20] respect to the ones based on thermal diffusion,[21–26] the intimate mechanisms governing the mechanochemical transformations are still a matter of debate.[6,7] This work attempts to clarify the role of localized mechanical stresses and of the associated excited states[6,7,9–20] by focusing on the early stages of the collision between two semicrystals of different metals. To this end, the behavior of semicrystals with surfaces of different roughness was studied under different impact conditions by means of molecular dynamics simulations. Systems, impact conditions, and numerical procedures are detailed in the following.

II. COMPUTATIONAL OUTLINE

Calculations were carried out on Ni and Zr semicrystals. These elements were selected due to the availability of reliable interatomic potentials and the capability of forming amorphous phases.[6,21] Different impact conditions were simulated by applying either a normal force or a combination of normal and tangential forces. In the former case, the compressive load pushed the two semicrystals each against the other. In the latter case, the colliding surfaces also underwent a sliding in opposite directions, thus experiencing a shear stress at collision.

A. Preparation of semicrystals

Ni and Zr semicrystals consisted of a stacking of atomic planes along the z Cartesian direction. Two different Ni systems with atoms arranged in the fcc cF4 structure were used. The former included 17 100 atoms arranged in a stacking sequence of 19 (110) planes. In the latter, the 17 100 atoms were instead arranged in a stacking sequence of 19 (111) planes. Both of these systems were employed in simulations involving plane surfaces, whereas only the latter was used in simulations concerning rough surfaces. The roughness was arbitrarily defined by employing the structural motif schematically depicted in Fig. 1(a). It consists of 120 atoms arranged on five atomic layers containing 61, 36, 19, 3, and 1 atoms, respectively. Two surfaces of different roughness were prepared by placing on the 19th atomic plane either one or four identical assemblies with random reciprocal orientation and positions. These were chosen in order to maintain the fcc (111) stacking sequence and avoid any contact between the assemblies. The two semicrystals with surface asperities consisted therefore of 17 220 and 17 580 atoms, respectively.

An analogous procedure was employed to create the Zr semicrystals with the characteristic hcp hP2 structure. Also for this element, two different systems were prepared. In the former case, the starting configuration consisted of 17 000 Zr atoms arranged in a stacking sequence of 34 (101) planes. In the second case, the starting configuration was instead

 ©2006 The American Physical Society

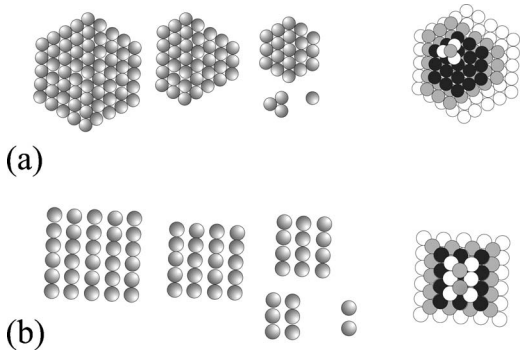

FIG. 1. A schematic depiction of the structural motifs (right) and their simple components (left) employed to model the surface of the Ni (a) and of the Zr (b) semicrystals. In the case of Ni, the atomic assembly includes 120 atoms. In the case of Zr, the structural motif is formed by 70 atoms.

formed by 18 125 Zr atoms arranged in a stacking of 29 (100) planes. Both the systems were employed in simulations involving plane surfaces, whereas only the latter was used in simulations concerning rough surfaces. The surface structure was modeled by means of the structural motif schematically illustrated in Fig. 1(b), consisting of 70 atoms arranged on five atomic layers containing 30, 20, 12, 6, and 2 atoms, respectively. A rough surface was prepared by randomly placing on the 29th atomic plane three assemblies. As in the case of Ni, positions and orientations were chosen in order to keep the underlying hcp (100) stacking sequence and avoid any contact between the assemblies. The Zr semicrystals with surface asperities contained then 18 335 atoms.

In all the different cases, the number of atoms per side of the semicrystals was selected in order to minimize the mismatch effects originating from the different size of the atomic species.

B. Interactions and simulation methods

Interatomic potentials were described by a semiempirical tight-binding force scheme based on the second moment approximation to the electronic density of states.[27,28] The repulsive part of the potential consists of a Born-Mayer pair-wise interaction, whereas the attractive part is expressed within the framework of the second moment approximation to the tight-binding band energy.[28,29] Interactions were computed within a cutoff radius approximately corresponding to the seventh shell of neighbors in Ni, which permits to satisfactorily reproduce thermodynamic and elastic properties.[27–30] The values of the potential parameters were taken from the literature.[27,28]

The equations of motion were solved by employing a fifth-order predictor-corrector algorithm[31] with a time step δt equal to 2.0 fs.

Periodic boundary conditions were applied along the x and y Cartesian directions. A "reservoir region" of seven atomic planes was defined along the z Cartesian direction at one end of each semicrystal, the free surface being located at the opposite end. Within each reservoir, the five atomic planes more distant from the free surface were considered "rigid," with their atoms occupying fixed positions defined by the ideal crystalline arrangement. The Nosè-Hoover thermostat[32] was applied to keep the temperature T constant at 300 K. The Parrinello-Rahman scheme was also implemented to properly deal with eventual shape changes of the elementary crystallographic cells.[33]

An initial equilibration stage at 300 K of 1 ns allowed for the single Ni and Zr semicrystals to separately relax. As expected, the atomic species at the free surfaces were the most mobile and underwent local displacements to attain the lowest possible potential energy. Such behavior is strictly connected with the atomic coordination number. Atoms with an equilibrium coordination have twelve nearest neighbors, whereas surface atoms have a coordination number dependent on their position. For example, Ni atoms on the plane (111) surface have nine nearest neighbors, whereas Ni atoms on the top of the surface asperities have a three-fold coordination. Analogous considerations can be made for the Zr atoms. The number of nearest neighbors determines to a great extent the potential energy experienced by the single atoms. Being the mobility of a given atom roughly proportional to its potential energy, the atoms with the lowest coordination number are expected to display the highest mobility. Due to the temperature considerably lower than the Ni and Zr equilibrium melting points T_m,[19,20] only short-range atomic displacements took place and even the surface asperities did not undergo significant morphological changes. This was also observed in independent simulations on Ni systems consisting of 17 150 atoms arranged in a stacking sequence of 14 (111) planes and equilibrated for 0.2 ns as well as on Zr semicrystals formed by 18 750 atoms arranged in 25 (101) planes and equilibrated for the same period.

After the equilibration stage, the Ni semicrystal was placed above the Zr one along the z Cartesian direction, as schematically illustrated in Fig. 2, at a distance of 0.4 nm. At such distance no significant interaction exists between the surfaces. An external constant force $F_{n,i}$, the intensity of which was selected in order to give the Ni system a center-of-mass velocity along the z Cartesian direction of about 10 m s^{-1}, was then applied to the i atoms in the Ni reservoir region.[10] Such impact velocity roughly reproduces the average impact velocity in ball mills.[6–8,34]

In some cases a tangential force F_t was also applied along the x Cartesian direction to simulate a shear stress[10] and obtain a couple of sliding. Correspondingly, opposite center-of-mass velocities of about 5 m s^{-1} were given to the Ni and Zr systems.[10]

As either the normal force or the combination of normal and tangential forces were applied, the Nosè thermostat was imposed only to the reservoir atoms to avoid the stochastic coupling with a thermal bath during the course of the impact. The spontaneous distribution of the kinetic energy over the colliding systems was thus evaluated. The atoms not located within the reservoir regions were left free to move according to Newton's equations of motion.[31]

The simulation time t was scaled to 0 at the beginning of the collision events. The impact events between the semicrystals began when a couple of Ni and Zr atoms approached to distances smaller than d_{NiZr}, the equilibrium distance between Ni and Zr atoms at 0 K.

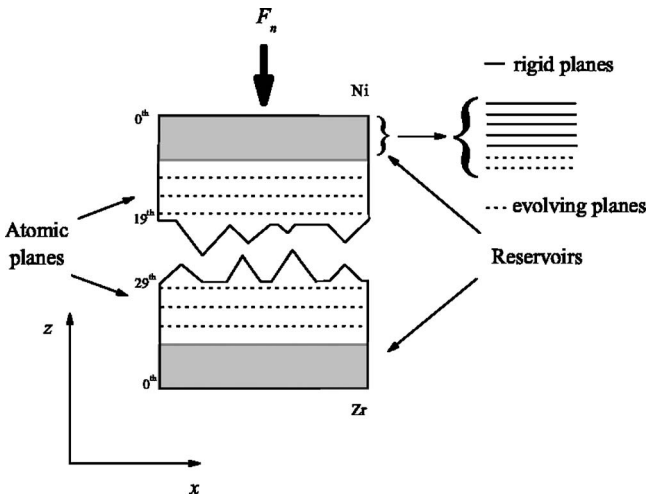

FIG. 2. A schematic illustration of the simulation box. The two "reservoir" regions are shown in gray at the borders of simulation cell along the z direction. The structure of reservoir regions is shown in detail to clearly indicate the five "rigid" atomic planes at the system border and the two atomic planes evolving according to normal dynamics. The rough free surfaces are also schematically shown together with the atomic planes. A normal force $F_{n,i}$ applies along the z Cartesian direction to the Ni semicrystal.

C. Analysis of atomic configurations

The long-range crystalline order in atomic planes was quantified by means of the planar static order parameter $S_p(\boldsymbol{k})$.[31] For an ideal crystal at 0 K, $S_p(\boldsymbol{k})$ equals unity for any wave vector $\boldsymbol{k}$. In a completely disordered plane it fluctuates instead near zero. $S_p(\boldsymbol{k})$ provides thus a direct quantitative measure of the degree of structural disorder. In the present case, it was evaluated with reference to the (111) and (110) crystallographic planes for Ni and the (100) and (101) ones for Zr. Surface asperities were not considered. The degree of order in slices including two or more atomic planes was evaluated by means of the three-dimensional static order parameter[31] $S(\boldsymbol{k})$ and the pair correlation function (PCF) $g(r)$.[31]

The rearrangement of atomic positions at impact was followed by looking at those atoms, hereafter referred to as defective, characterized by a defective coordination. A defective atom is here defined as an atom with a number of nearest neighbors different from twelve. A distance criterion was adopted to evaluate the number of nearest neighbors. In particular, two atoms were regarded as nearest neighbors when located at distances smaller than the one, r_m, corresponding to the first minimum in the PCF. Surface atoms, which necessarily have an incomplete coordination shell and then an intrinsic defective coordination, were not considered. Defective atoms formed relatively complex aggregates, hereafter referred to as clusters. Their number N_{cl} and size n were evaluated by regarding two defective atoms as connected when located at distances shorter than r_m.

The distance criterion can be safely applied to pure Ni and Zr phases, which possess characteristic $r_{m,Ni}$ and $r_{m,Zr}$ length scales. However, a further length scale $r_{m,mix}$ appears when Ni and Zr atoms mix at the interface under the action of local shear stresses. It corresponds to the first minimum of the PCF of the region involved in the mixing process.

The shear induced processes of lattice perturbation and atomic displacement were further characterized by identifying the "force chains," here defined as ensembles of atoms interacting with repulsive forces. In order to roughly discriminate between repulsive interactions originated from thermal fluctuations and local shear stresses, a threshold force intensity f_r was employed. An interatomic distance r_r was correspondingly identified for the different Ni-Ni, Ni-Zr, and Zr-Zr pair interactions. The threshold distance r_r was equaled to r_{av}-3σ, where r_{av} and σ represent the average position and the standard deviation of the Gaussian function best fitting the first peak of the suitable partial PCF. A force chain is then formed by atoms located at distances shorter than r_r.

Any force chain has characteristic size and shape, which correspond respectively to the number n_{fc} of atoms involved in the force chain and their spatial arrangement. n_{fc} and the number N_{fc} of force chains can be evaluated by regarding two atoms as involved in the same force chain when located at a distance shorter than r_r. A quantitative characterization of the spatial arrangement of atoms in force chains, i.e., an approximate estimation of the average fractal dimension d_f, was obtained by taking advantage of the relationship between the force chain size, n_{fc}, and its length, L_{fc}. This latter quantity represents the maximum distance between two atoms in a given force chain.[35]

D. Impact configurations

Various collision events were simulated by employing surfaces with different roughness under different impact conditions. The semicrystals will be hereafter identified according to the morphology of their surface. The list of impact configurations investigated is reported below:

1. plane (111) Ni surface—plane (100) Zr surface;
2. plane (110) Ni surface—plane (101) Zr surface;
3. (111) Ni surface with 1 asperity—plane (100) Zr surface;
4. (111) Ni surface with 4 asperities—(100) Zr surface with 3 asperities.

Except for the latter configuration, calculations were carried out with the normal force only as well as with the combination of normal and tangential forces. Seven different cases were therefore studied, which will be separately discussed for the sake of clarity.

III. COLLISION EVENTS BETWEEN PLANE SURFACES

As mentioned before, the impacts between the (111) Ni and (100) Zr surfaces as well as between the (110) Ni and (101) Zr surfaces were studied with and without a shear component in addition to the compressive load.

A. Collision events without shear component

The collision of Ni and Zr semicrystals with plane surfaces approaching along the z Cartesian direction without relative sliding along the x Cartesian direction represents the

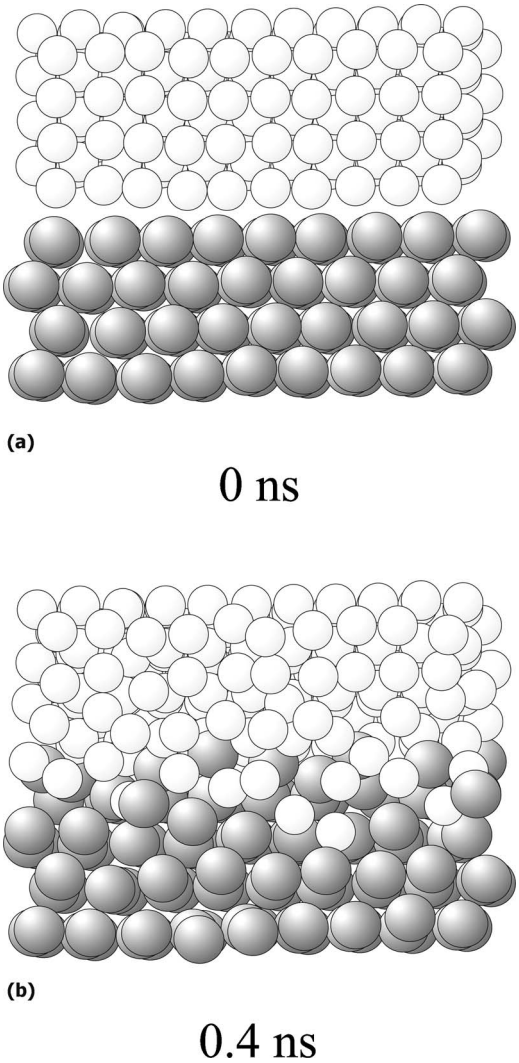

FIG. 3. Snapshots of the (111) Ni–(100) Zr interface immediately before the impact (a) and after 0.4 ns (b). Only the atomic species within a slice about 1 nm thick at the center of the simulation cell are shown for sake of clarity. The Ni and Zr atoms are reported respectively in light and dark gray. It can be seen that mixing processes involve a limited interfacial region.

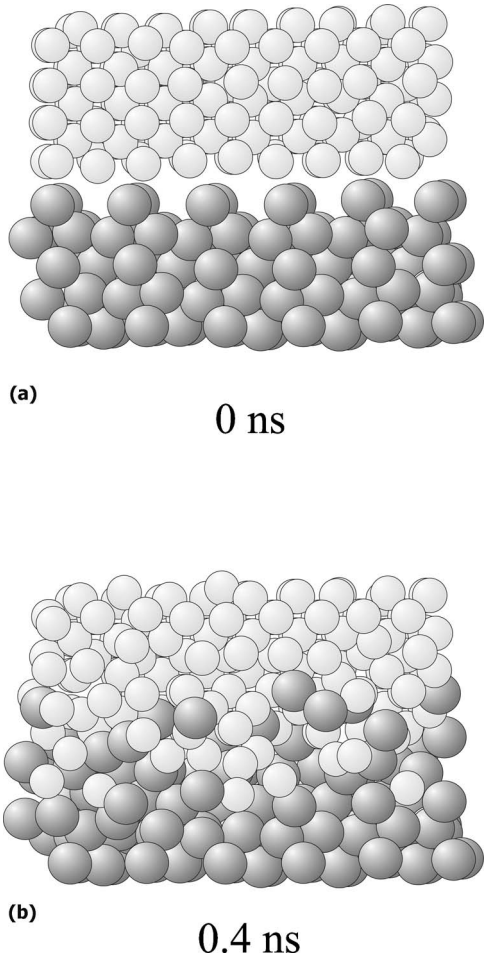

FIG. 4. Snapshots of the (110) Ni–(101) Zr interface immediately before the impact (a) and after 0.4 ns (b). Only the atomic species within a slice about 1 nm thick at the center of the simulation cell are shown for sake of clarity. The Ni and Zr atoms are reported respectively in light and dark gray. The intermixed layer thickness is larger than in the (111) Ni–(100) Zr interface case.

simplest impact event investigated in the present work. Independent of the topology of the impacting surfaces, no significant atomic mixing took place at the interface. This can be seen from Fig. 3, where snapshots of the (111) Ni-(100) Zr interface immediately before the impact and after 0.5 ns are shown. Only four atomic planes at the interface are affected by atomic displacement processes induced by the compressive load. These planes display approximately the same values of the static order parameter $S_p(\boldsymbol{k})$, amounting to about 0.5, after 0.5 and 1 ns. All the other planes are instead characterized by $S_p(\boldsymbol{k})$ values on the order of 0.8. This suggests that surface atoms are involved in fast rearrangement processes only at the very early stage of the collision, whereas successively the system enters a sort of "jammed" state in which significant atomic displacements are no longer possible. An analogous behavior was observed at the impact between the (110) Ni and (101) Zr surfaces. The snapshots of the interface immediately before the collision and after 0.4 ns reported in Fig. 4 point out however that the disordering processes involve a larger number of atomic planes. This suggests that the surfaces with less dense packing undergo more extended atomic position rearrangements. However, also in this case the system rapidly attains a state of structural arrest. The rationale for such behavior lies in the roughly uniform distribution of the compressive load over the whole surface area. The load induces indeed a uniform compression of the interplanar distances. This prevents the formation of force chains and therefore the occurrence of local shear events, as will be shown in the following, to induce extensive rearrangements of the atomic positions.

B. Collision events with shear component

The situation drastically changes when a tangential force along the x Cartesian direction is added to the normal force along the z Cartesian direction. The relative sliding of the approaching semicrystals gives rise to a shear stress at im-

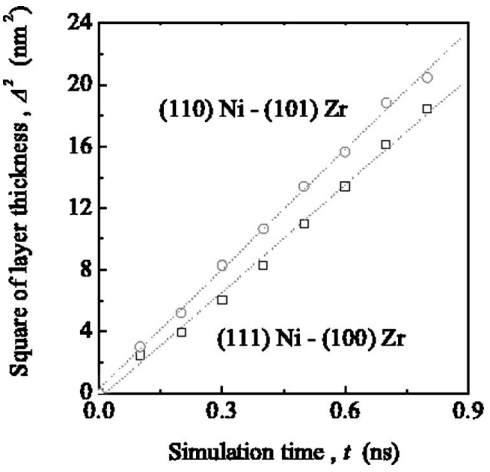

FIG. 5. The square of the intermixed layer thickness, Δ^2, as a function of time t for the Ni (111)–Zr (100) and Ni (110)–Zr (101) interfaces. The time dependence of the layer thickness is similar to the one observed under thermal diffusion conditions. Best-fitted lines are also quoted.

pact. Under such conditions, the system evolves according to a dynamics essentially analogous to the one characterizing atomic mixing and chemical disordering processes in crystalline systems under shearing.[19,20] For this reason and for the sake of brevity, the mechanistic features of shear-induced processes here observed will be only briefly described. A detailed discussion can be found in previous contributions.[19,20]

Under the action of shear stresses, the approximately planar interface formed at impact undergoes a gradual roughening accompanied by a local distortion of the crystalline lattices. Distortions increase with time and induce the mixing of Ni and Zr at interface. Chemical disordering is soon accompanied by a local loss of structural order and a disordered layer appears. Its thickness Δ along the z Cartesian direction, evaluated as the difference between the z coordinates of the Ni and Zr atoms respectively closer to the Zr and Ni reservoirs, increases with the simulation time. Figure 5 clearly indicates that Δ scales linearly with the square root of time both in the case of a (111) Ni–(100) Zr and of a (110) Ni–(101) Zr interface. The rate of amorphous layer thickness increase is higher for the (110) Ni–(101) Zr interface. Mixing is governed by apparently random processes dependent on the distortion of local atomic configurations and the formation of atoms with defective coordination below the surfaces, which undergo continuous rearrangement processes. These evidences suggest that the mixing process and the related loss of structural order are mechanically-driven processes, with thermal contributions playing a secondary role.

IV. COLLISION EVENTS BETWEEN SURFACES WITH SMALL ROUGHNESS

The collision event between a (111) Ni surface with a single asperity and a plane (100) Zr surface is the prototypical case of impact between surfaces with small roughness. The impact initiates when and where the Ni asperity enters into contact with the plane Zr surface.

A. Collision event without shear component

The atoms at the point of local contact between the Ni asperity and the plane Zr surface experience a sudden mechanical load. The high local pressure due to the roughly pyramidal geometry of the asperity gives rise to intense shear stresses that determine, in turn, the rapid accumulation of atomic strain. The latter is at least partially relieved by either net atomic displacements or rearrangements of coordination shells. These processes become evident from the direct visualization of the atomic configurations at the point of contact, quoted in Fig. 6 at different times. Both Ni and Zr atoms rapidly modify their positions in response to local shear stresses and the consequent mass transport processes occur under ballistic conditions. The intensity of forces is such that a small number of atoms is also temporarily projected into the vapor phase. Atomic mixing processes also take place independent of thermal diffusion.

The sudden mechanical load induces a considerable increase of the kinetic energy of the Ni and Zr atoms involved in the collision event since the first contact. A local rise of the temperature T therefore occurs. Of course, the instantaneous and local temperatures do not correspond to the equilibrium temperature defined by the zeroth principle of thermodynamics.[36] Detailed information on the temperature rise was obtained by evaluating the kinetic energy distributions of surface atoms. These were defined for Ni as the atoms belonging to the 19th plane or located between it and the 29th plane of the Zr semicrystal. For Zr, the surface atoms were similarly defined as the atoms belonging to the 29th atomic plane or located between it and the 19th plane of the Ni semicrystal. Ni and Zr surfaces were then divided into a grid of 144 cells and the instantaneous temperature of each cell evaluated by averaging over the kinetic energy of the atoms located within the cell. The surface temperature distributions observed at different times are shown in Fig. 7. It can be seen that the temperature values are remarkably higher in the region of contact between the Ni asperity and the Zr plane surface. The kinetic energy of the atoms directly involved in the collision event and of their neighbors undergoes a marked increase as the impact proceeds. The local shear stresses determine the enhancement of the mobility of an increasing number of surface atoms and local temperatures on the order of 1900 K are attained. Such values are respectively about 300 and 100 K above the estimated Ni and Zr T_m values.[19,20] Accordingly, the small volumes within which the temperature exceeds the melting point could be regarded as molten. The melting process is however not only local, but also transient, given that the high temperatures are observed for times on the order of 20 ps. The local failure of the crystalline arrangement is thus not a consequence of thermal phenomena, but rather a result of the shear-induced localization of kinetic energy.

1. Defective atoms and lattice defects

When the Ni asperity impinges on the plane Zr surface, the underlying atoms are rapidly involved in localized rearrangement processes. The associated increase of structural disorder, monitored by means of the planar static order parameter $S_p(\boldsymbol{k})$, propagates along the z Cartesian direction at a

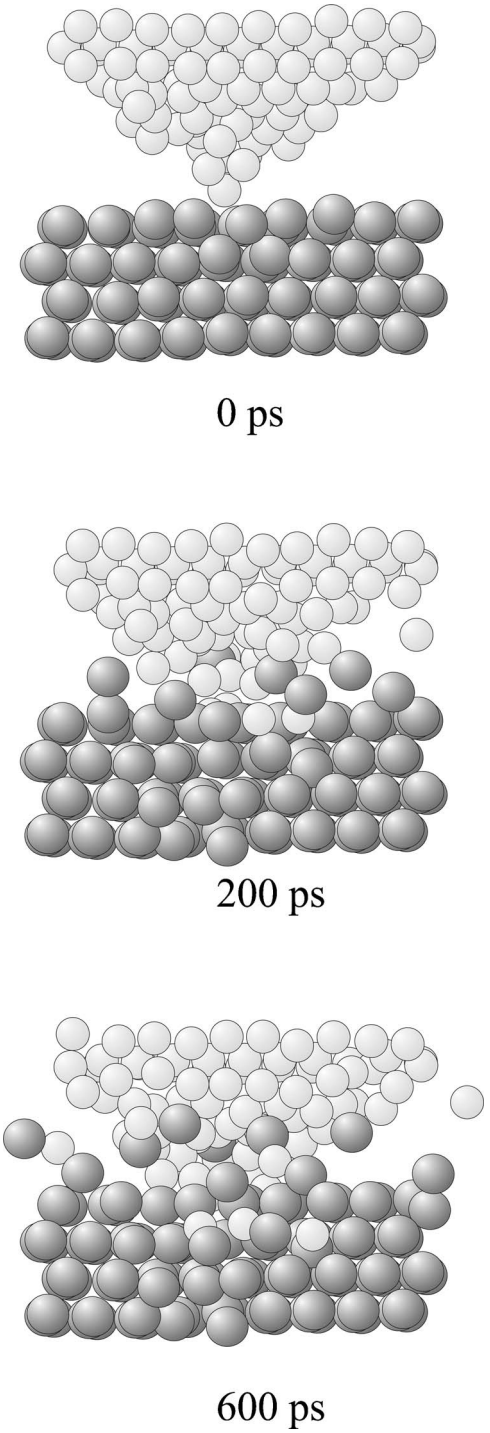

FIG. 6. Snapshots of the Ni asperity colliding with the plane Zr surface at the different times quoted. The Ni asperity is deeply modified by the action of local shear stresses. A small number of atoms is also projected in the vapor phase. Mixing phenomena induced by the severe rearrangement of atomic positions are also evident.

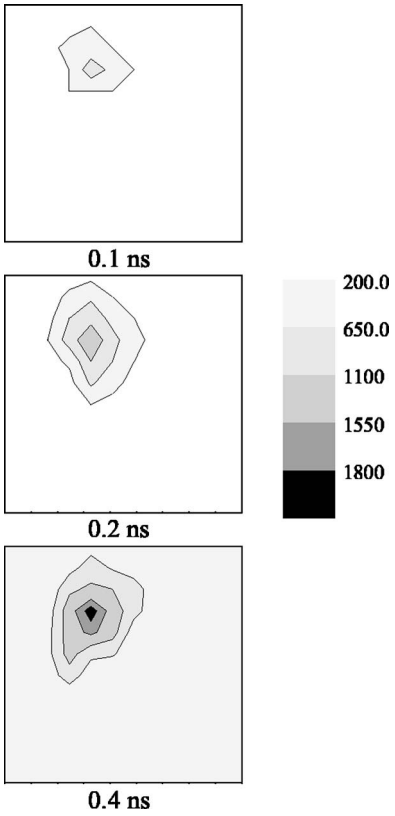

FIG. 7. The temperature distribution at the interface between the Ni and the Zr semicrystals at the different times quoted. The highest temperature is attained in correspondence of the asperity at the Ni surface. Local temperatures as high as 1900 K are observed. The temperature coding with gray levels is also shown.

rate of about 70 m s^{-1}. The gradual disordering, marked by the drop of $S_p(\boldsymbol{k})$ values below 0.8, is due to the formation of atoms with defective coordination. Ni defective atoms were identified in the region between the 6th and 18th atomic planes, whereas Zr defective atoms in the region between the 6th and 28th planes. Defective atoms form via a local rearrangement of the coordination shells of two neighboring atoms, which gives rise to a pair of atoms with 11- and 13-fold coordination respectively. Other defective coordination numbers are rarely observed and, in any case, for times on the order of only 0.1 ps. The first defective atoms on the Ni and the Zr sides appeared in the 18th Ni and the 28th Zr atomic planes, respectively after about 3.2 and 4 ps, in correspondence of the Ni asperity. Starting from such a point, the defective atoms successively spread over extended regions of the semicrystals.

A direct visualization of defective atoms in both Ni and Zr semicrystals points out that such species arrange according to stringlike structures as the one shown in Fig. 8. The number of defective atoms in a given cluster and its position continuously change during the course of the impact event as a consequence of the enhanced atomic mobility under shearing. The cluster dynamics is mainly governed by branching chain processes that can in principle involve both the ramification of a single cluster as well as the approach and final intersection of two different clusters. The former process predominates in the present case.

Branching-chain processes occasionally induce the formation of closed loops of defective atoms such as the one shown in Fig. 9. Such loops, with lifetimes on the order of 20 ps, roughly correspond to Shockley partial dislocations

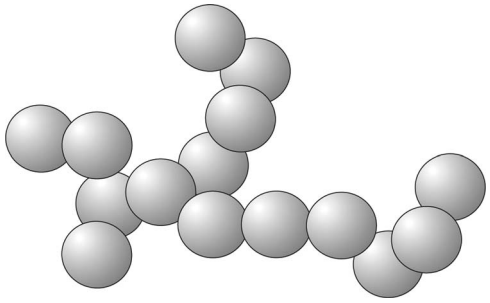

FIG. 8. A cluster of 15 Zr atoms with defective coordination. The snapshot refers to the atomic configuration at 60 ps. The atoms display a stringlike arrangement. For the sake of clarity, only the atomic species belonging to the cluster are shown.

surrounding stacking faults.[37] The loops on the Ni side of the Ni-Zr interface are seen to glide mainly along the [101] and [110] crystallographic directions. On the Zr side of the interface, the loops glide instead mainly along the [110] and [210] crystallographic directions. It seems therefore that such loops move in accordance with the known systems of gliding in fcc and hcp lattices. The results on this point are however only preliminary and further work is required to explore in detail the configurations of defective atoms at the various stages of the impact event.

2. Force chains

The appearance of defective atoms at the beginning of the impact event and their subsequent proliferation in both the Ni and Zr semicrystals is a consequence of the propagation of the mechanical deformation from the surface to the bulk. The impact involves initially one Ni atom and two Zr ones. In response to the accumulation of strain, the atoms move in order to relieve the strain and lower their potential energy. The atomic displacement from lattice positions induces a marked rearrangement of coordination shells. In a very short time, a certain number of atoms become involved in analogous rearrangement processes and a part of them interact with repulsive forces higher than f_r at distances shorter than r_r. Such atoms form a "force chain." Given that the collision event begins at a single point of contact, a single force chain originates at such point. The atomic configurations of the force chain at three different times are shown in Fig. 10. It can be seen that the number of Ni and Zr atoms involved increases as the distance between the semicrystals decreases. During this stage, the force chain undergoes branching chain processes and after about 0.3 ns the number of atoms involved amounts to about 1500. Their arrangement has clear fractal features. The relationship between n_{fc} and L_{fc} allows for approximately estimating the average fractal dimension d_f of the force chain. Figure 11 indicates that the ln-ln plots of L_{fc} as a function of n_{fc} at three different times are roughly linear. This means that such quantities obey a power-law relationship $L_{fc} \sim n_{fc}{}^{\nu}$. ν represents the average slope of the linear trends in Fig. 12 and amounts approximately to 0.98, 0.91, and 0.76, respectively after 0.1, 0.2, and 0.3 ns. Accordingly, the fractal dimension $d_f \sim \nu^{-1}$ of the force chain amounts to about 1.02, 1.10, and 1.31. The force chain evolves from an essentially linear arrangement to a more complex one.[35]

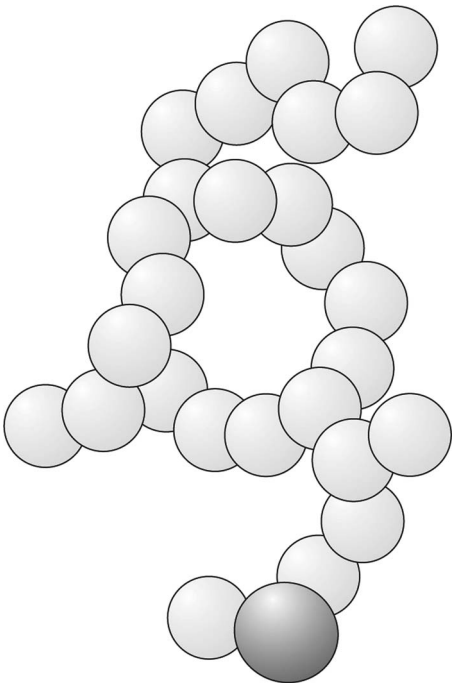

FIG. 9. A cluster of 26 Ni atoms with defective coordination containing a closed loop. The cluster refer to the atomic configuration at 130 ps. For the sake of clarity, only the atomic species belonging to the cluster are reported. A Zr atom, also connected to the cluster, is quoted in heavy gray. Ni atoms are reported in light gray.

The comparison between the positions of defective atoms and of the ones involved the force chain indicates a strong correlation between the two ensembles of atoms. This is a widely expected result, given that the rearrangement of coordination shells giving rise to defective atoms is due to the propagation of force chains in the bulks. Each atom becomes involved in a force chain at times dependent on its distance from the point of first contact between the colliding surfaces, i.e., farther atoms are involved later. Once a given atom has become involved in a force chain, it can also escape from it by undergoing a displacement to a position in which the local strain is almost completely relieved. The length of the time intervals during which a given atom is involved in a force chain changes irregularly.

3. The mixing process at the interface

As discussed in detail above, the force chain involves both Ni and Zr atoms. The atomic displacements associated and the consequent generation of defective atoms promote the occurrence of mixing processes in the interfacial region close to the Ni asperity. The characteristic size Δ of the region in which the chemical species intermix, which measures the distance of penetration of the atoms of one species into the lattice of the other, changes with time as shown in Fig. 12 where Δ^2 is quoted as a function of t. The first portion of the curve is remarkably linear. This suggests that during the early collision stage the size of the intermixed region displays a time dependence analogous to that of conventional

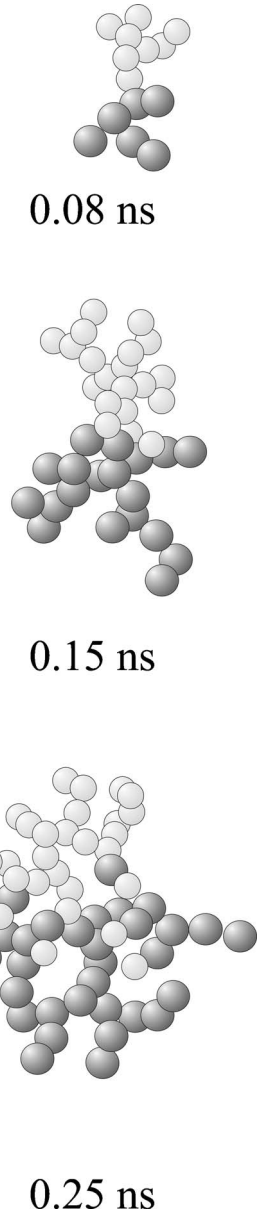

FIG. 10. The atomic configuration of a force chain at the three different times indicated. The force chain originates at the point of first contact between the Ni asperity and the plane Zr surface. Both Ni and Zr atoms, respectively reported in light and dark gray, are involved. The size of the force chain as well as the number and extension of the ramifications increase with time.

thermal diffusion.[19,20] A definite change of slope is observed after about 0.40 ns, probably indicating a change in the mechanism governing the mixing process. This conjecture is supported by the evidence that at about 0.32 ns the two colliding semicrystals have attained the configuration in which the asperity at the Ni surface is strongly interacting with the Zr surface. At about 0.40 ns, the surface structures have been already significantly perturbed and the system is approaching the configuration in which the two Ni and Zr semicrystals strongly interact over the whole interface area. Under such circumstances, the mobility of the surface species is greatly reduced. The mechanism of ballistic displacement of Ni and

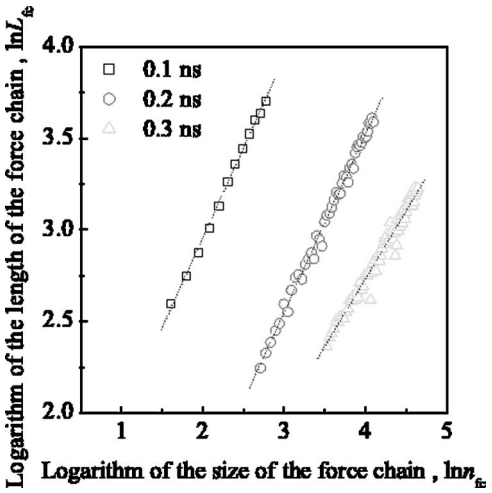

FIG. 11. The ln-ln plot of the length L_{fc} of the force chain as a function of its size n_{fc}. The plots refer to the three different times quoted. The rough plot linearity indicates that L_{fc} and n_{fc} obey a power-law relationship $L_{fc} \sim {n_{fc}}^{\nu}$, where ν represents the average slope of the linear trends. The slope ν changes with time and takes the values 0.98, 0.91, and 0.76.

Zr surface atoms at the surface is then gradually replaced by processes involving a slower rearrangement of the atomic positions. As a result, while the size Δ of the intermixed region amounts to about 3 nm after 0.42 ns, it has increased approximately of only 1 nm after additional 0.5 ns. The intermixed region, which also displays a certain degree of structural disorder, consists of about 400 Ni atoms and 300 Zr ones.

4. The relaxation process

As the simulation proceeds, both force chain and defective atoms gradually approach the reservoir regions containing immobile species. This fact can result in a nonphysical

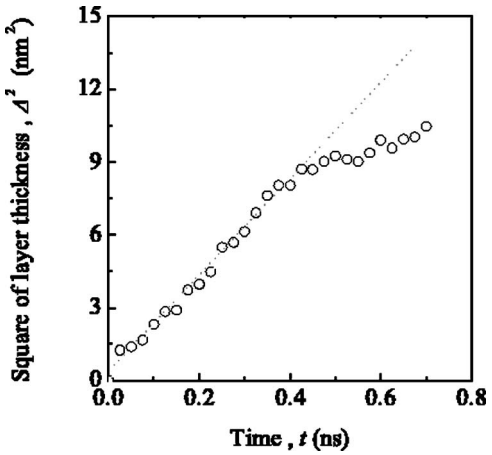

FIG. 12. The square of the intermixed layer thickness, Δ^2, as a function of the time t. The curve obtained can be divided into two approximately linear portions. The time dependence of the distance over which mixing phenomena occur at impact is therefore similar to the one of thermal diffusion. The line best fitted to the first portion is also shown.

evolution of the system and therefore a wrong simulation of the atomic scale processes taking place at collision. For this reason, the calculations were stopped when one of the mobile atoms in the reservoir was involved in a force chain. This typically took place after about 1 ns.

In order to gain information on the possible dynamics of the relaxation processes relieving the strain of local atomic configurations in absence of mechanical loads, the normal force compressing the semicrystals was removed. This produced a decrease of n_{fc} of roughly the 80% in about 70 ps. A certain number of highly strained configurations relaxed on longer times, on the order of 240 ps. After about 0.1 ns, no force chain was detected within the system.

The relaxation process was seen to occur via short-range displacements of atomic species rarely exceeding a distance of about 0.4 nm. This means that such processes essentially involved the coordination shells. However, the system is not able to completely remove local strains and rearrange high-energy configurations. This is mostly a consequence of the Nosè-Hoover thermostat applied to the mobile atoms in the reservoir regions, which removes the excess kinetic energy at interface in times of the order of 0.1 ns. After 60 ps since the removal of the normal force the apparent temperature of the interfacial region, evaluated by averaging over five atomic planes below the surface on both the Ni and Zr sides, dropped from about 800 K to about 500 K. After additional 60 ps, the interface temperature was only 70 K higher than 300 K. Under such circumstances, the atomic mobility is greatly limited and long-range displacements prevented. An approximately spherical region about 3.5 nm in size, located in correspondence of the original Ni asperity, maintains thus a disordered structure.

B. Collision event with shear component

The atomic-scale processes at the impact between the (111) Ni surface with a single asperity and the plane (100) Zr surface change drastically when the surfaces slide in opposite directions. The reasons underlying the different behavior are connected with the modifications of the surface morphology at impact, evident in Fig. 13 where snapshots of the atoms at the Ni and Zr surfaces are reported for different times. The relative sliding determines a gradual wear of the Ni asperity, with consequent damage of the Zr plane surface. A scratching process starts as the asperity impinges on the Zr surface. A small track appears along the sliding direction due to the interaction with the Ni asperity. Some Zr atoms are displaced from their initial position and pushed forward, whereas Ni atoms initially belonging to the asperity are left behind. A disordered mixing of Ni and Zr atoms takes place during the first stages of the collision, until the Ni asperity is not completely erased. Once the contact between the Ni and Zr surfaces involves the whole area, the system evolves as in the case of two plane surfaces colliding in presence of a shear component. The mechanistic scenario is analogous to the one already discussed and will not be described here for the sake of brevity.

V. COLLISION EVENTS BETWEEN SURFACES WITH LARGE ROUGHNESS

The impact between a (111) Ni surface with four asperities and a (100) Zr surface with three asperities is an example

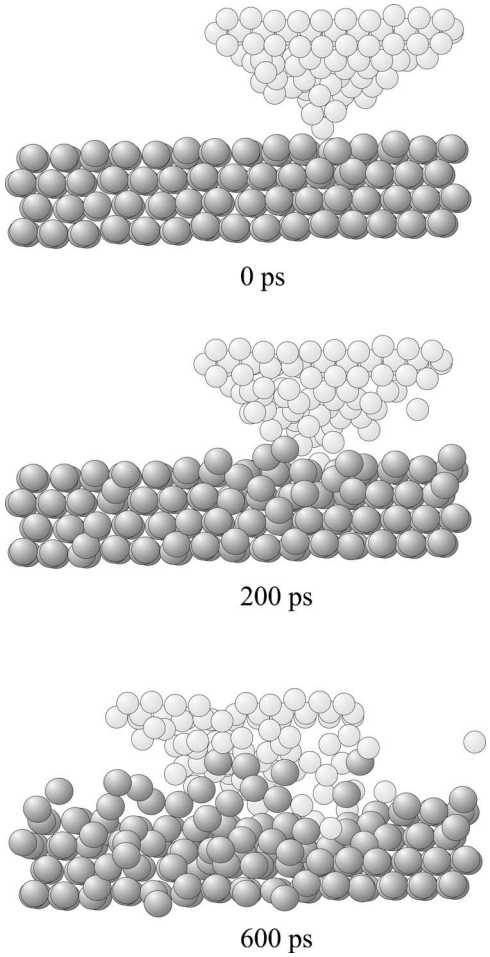

FIG. 13. The surface morphology during the collision event with shear component between a (111) Ni surface with a single asperity and a plane (100) Zr surface. The snapshots at the times quoted indicate that the impinging asperity roughens the Zr surface. A fraction of Ni atoms, in light gray, is deposited on the perturbed Zr surface. Some Zr atoms, in dark gray, are instead pushed forward by the Ni asperity.

of collisions between surfaces with a high degree of roughness. Such a roughness on the nanometer scale is of course quite improbable from an experimental point of view. However, it gives rise to a relatively large number of local mixing events the study of which could equally provide useful information on the atomic-scale dynamics of localized shear events. It is within this framework that the present simulation should be considered.

The surface patterns obtained at the end of the initial equilibration stage are shown in Fig. 14. Two of the four Ni asperities are located approximately in coincidence with two of the three Zr asperities. The first contact between the Ni and Zr semicrystals at impact occurs therefore in correspondence of these asperities. The elementary processes taking place at impact are similar to the ones observed in the previous case. The sudden mechanical loads developing at the points of contact generate intense shear stresses that induce the modification of local atomic configurations. As shown in Fig. 15, where snapshots of the colliding asperities are reported at different times, the atoms are displaced from their

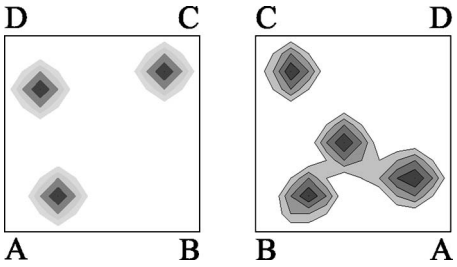

FIG. 14. The surface structure of Ni (right panel) and Zr (left panel) semicrystals. A density level map is used for the sake of clarity. The surface edges are indexed with letters to facilitate the correct superposition of the semicrystals, which in the simulation cell are reciprocally oriented in order that the same letters superpose when the surfaces are each in front of the other.

initial positions under ballistic conditions. This results in the increase of their kinetic energy, mirrored by a corresponding increase of the temperature T as well as in the rapid mixing of atomic species. The distributions of the Ni and Zr surface temperature, obtained as in the previous case by considering only surface atoms and dividing the surface into a grid of 144 cells, are quoted in Fig. 16. As expected, the temperatures of the regions of first contact are considerably higher than the ones in the rest of the surface. Local temperatures as high as 2100 K can be attained even though for short time periods.

A. Defective atoms and lattice defects

The values of the planar static order parameter $S_p(\boldsymbol{k})$ indicate that the mechanical deformation gradually propagates along the z Cartesian direction at a rate of about 100 m s^{-1}. As discussed in detail in the previous case, the disordering process is due to the formation of defective atoms. The first defective atoms appeared in correspondence of the asperities undergoing the first contact after about 2.4 ps on the Ni side and after about 3 ps on the Zr side. The defective atoms spread successively over more extended regions, attaining a more uniform distribution. They arrange according to string-like structures undergoing a continuous change of size and position. Branching-chain processes occur according to the two different mechanisms previously indicated. Given that in the present case the impact involves surfaces with large roughness and various clusters of defective atoms are generated, branching-chain processes mainly consist of the intersection of such clusters.

B. Force chains

Due to the particular configuration of their free surfaces, the collision between the rough Ni and Zr surfaces begins at two points of contact. Two separate force chains are correspondingly generated. When the proper distances are attained, two other points of contacts between the semicrystals are established and two other force chains appear. After about 4.3 ps, the system contains four force chains. Two of them are relatively large and ramified, consisting respectively of 1437 and 1645 atoms. The others are considerably

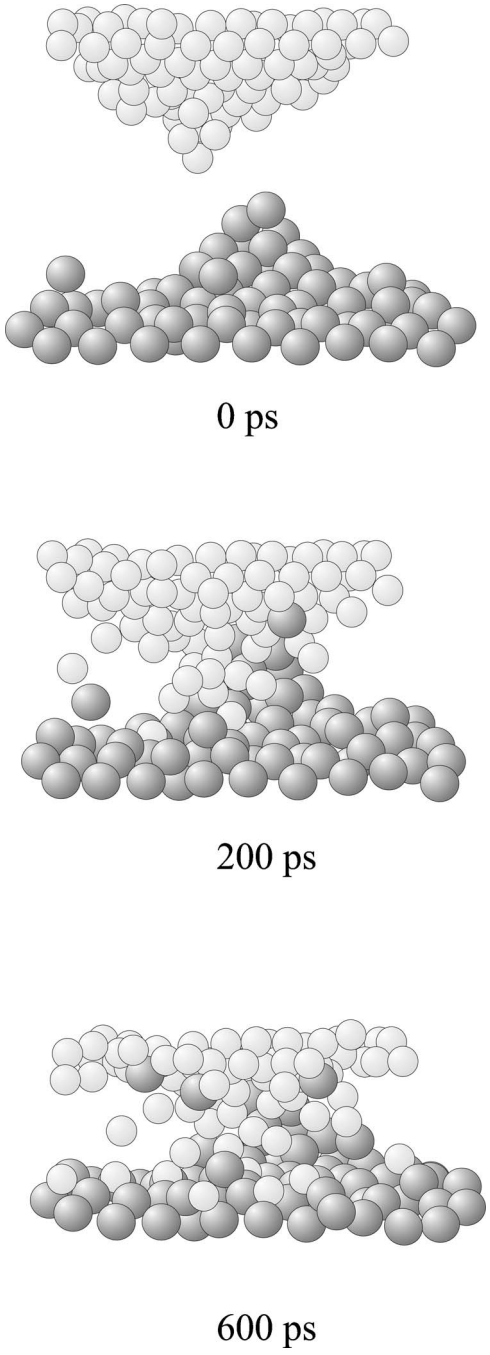

FIG. 15. Two colliding asperities at the surfaces of the Ni and Zr semicrystals at the different times quoted. The atomic assemblies are drastically modified during the impact. The atoms are heavily displaced from their positions by the action of local shear stresses. A few atoms are also projected in the vapor phase. The atomic position rearrangements also induces mixing phenomena.

smaller, about 100 atoms each. As the impact event proceeds, the size of the force chains as well as the volume they span increase. After about 0.5 ns, one of the force chains originated at the first point of contact ramifies toward a smaller one and finally intersects it. The two force chains then merge in a single one. Analogous coalescence processes take place successively, so that only one force chain is observed after about 0.7 ns. These processes are partially illustrated by the

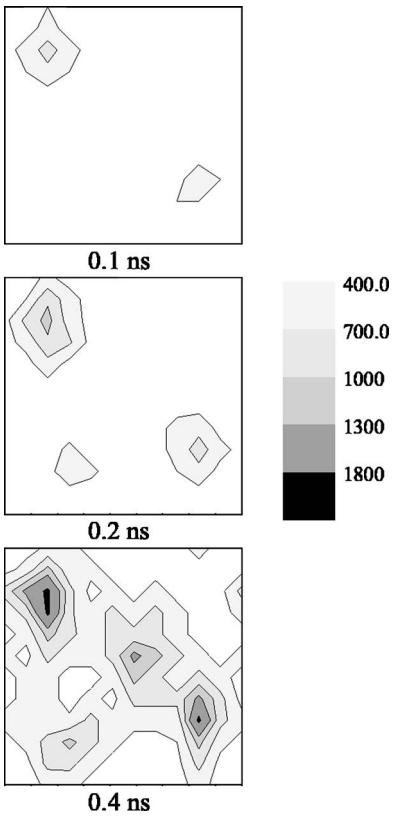

FIG. 16. The temperature distribution at the interface between the Ni and the Zr semicrystals at the different times quoted. The highest temperatures are attained in correspondence of the atomic assemblies at the surface. Local temperatures as high as 2100 K are observed. The temperature coding with gray levels is also shown.

configurations of one of the force chains shown in Fig. 17 at three different times. The data quoted in Fig. 18, reporting the roughly linear ln-ln plots of the force chain length L_{fc} as a function of the force chain size n_{fc} at three different times, indicate that also in the present case L_{fc} and n_{fc} obey the power-law relationship $L_{fc} \sim n_{fc}^{\nu}$ Three different linear arrangements are obtained at the three different times considered, with the slopes ν approximately amounting to 1.01, 0.86, and 0.62. Accordingly, the fractal dimension $d_f \sim \nu^{-1}$ amounts to about 1, 1.2, and 1.6. Therefore, the force chain evolves from a linear arrangement to a structure resembling the one of a self-avoiding random walk.[35]

C. The mixing process at the interface

The large surface roughness determines the occurrence of mixing phenomena between the chemical species at a rate larger than the one observed in the previous case. The square of the thickness Δ of the intermixed layer is reported in Fig. 19 as a function of the time t. Two dynamical regimes can be easily identified in the plot. During the first stages of the impact Δ displays a time dependence analogous to the one pertaining to conventional thermal diffusion processes. As in the previous case, a definite change of slope is observed after about 0.35 ns. A change in the mechanism governing the mixing process takes place after about 0.3 ns, when all the

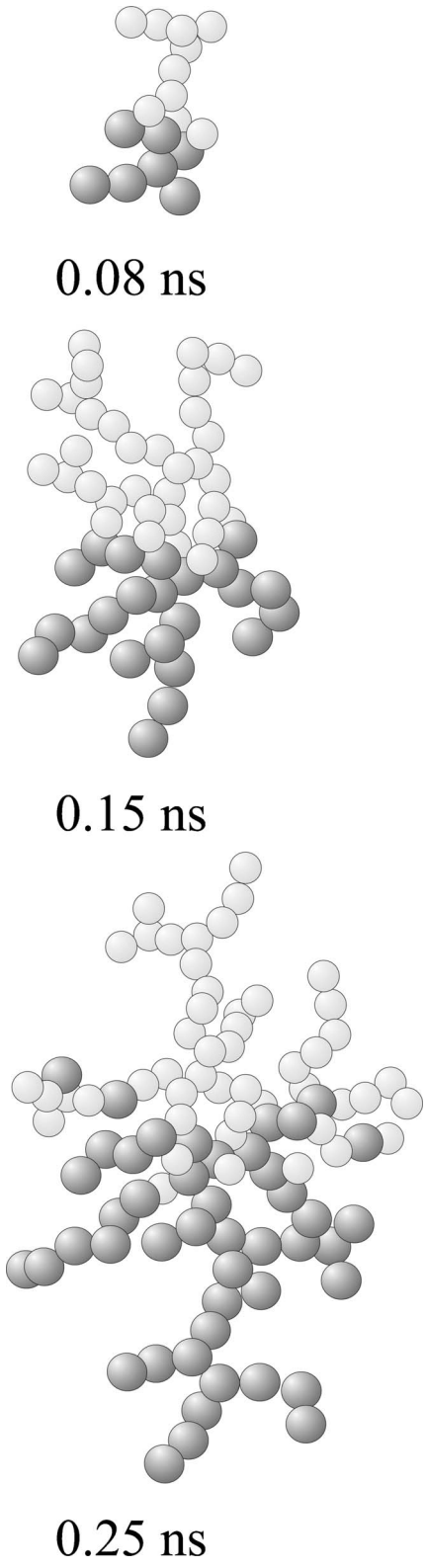

FIG. 17. The atomic configuration of a force chain at the three different times indicated. The force chain originates at one of the points of first contact between the Ni and Zr asperities. Ni and Zr atoms are reported respectively in light and dark gray. The size of the force chain as well as the extension of its ramifications increase with time.

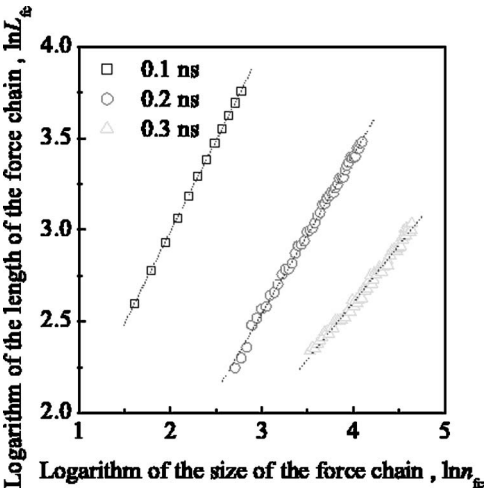

FIG. 18. The ln-ln plot of the average length L_{fc} of the force chain as a function of its size n_{fc}. The plots refer to the three different times quoted. L_{fc} and n_{fc} obey a power-law relationship $L_{fc} \sim {n_{fc}}^{\nu}$, where ν represents the average slope of the linear trends. The slope ν changes with time and assumes the values 1.01, 0.86, and 0.62.

asperities at the surfaces are strongly interacting with each other or directly with the surface of the opposite semicrystal. After about 0.35 ns, the two semicrystals experience an intense compressive load that induces a change of the atomic rearrangement conditions from ballistic to less energetic ones. This results in turn in a decrease of the rate with which the disordered layer thickness increases.

D. The relaxation process

After about 0.7 ns, defective atoms and force chains approach the reservoir regions. To avoid any unphysical behavior, the normal force was then removed and the system left free to relax. The relaxation processes relieve the strain of

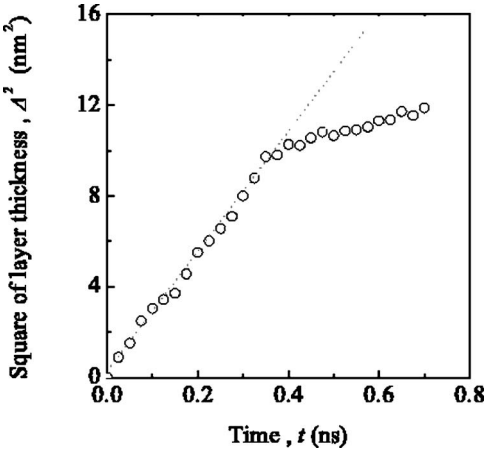

FIG. 19. The square of the intermixed layer thickness, Δ^2, as a function of the time t. Two approximately linear portions are observed. The time dependence of the distance over which mixing phenomena occur at impact is similar to the one of thermal diffusion. The line best fitted to the first portion is also shown.

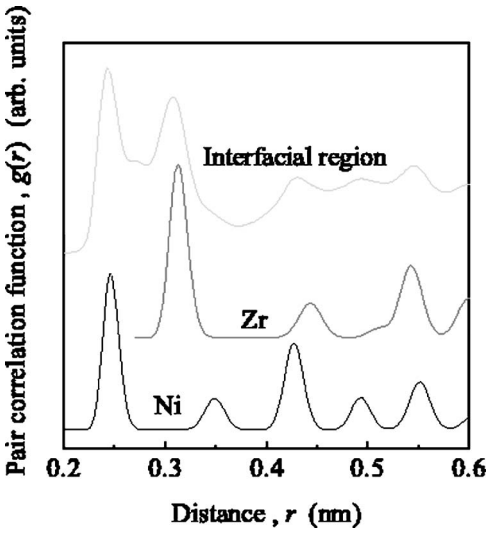

FIG. 20. The global PCF $g(r)$ of the interfacial region between the 14th Ni plane and the 24th Zr one after about 0.6 ns since the removal of the normal force. The PCFs $g(r)$ of Ni and Zr bulk systems at 500 K are also reported for the sake of comparison. The evident crystalline peaks are superposed to two broad halos indicative of structural disorder.

local atomic configurations, determining the disappearance of the force chain within approximately 0.1 ns by successive rearrangements of the coordination shells. Long-range atomic displacements are prevented by the Nosè thermostat, which removes the excess kinetic energy at the interface within time intervals on the order of 0.1 ns. Under such circumstances, the disordered layer at the interface does not disappear. The PCF of the interfacial region quoted in Fig. 20 shows that such layer possesses an amorphouslike structure. The disordered layer consists of about 5000 Ni atoms and 3500 Zr ones.

VI. CONCLUDING REMARKS

The evidences hitherto discussed suggest that a collision event at relatively low initial temperatures determines a complex sequence of atomic scale processes. The behavior of the crystalline systems at impact is strongly dependent on the topology of the colliding surfaces. Plane surfaces experiencing a compressive load do not give rise to significant mixing and soon after the impact the system experiences a structural arrest. Such structural arrest is not observed in collisions involving either rough surfaces or plane surfaces relatively sliding.

In the case of collisions between rough surfaces, the impact event involves initially the surface asperities. At the points of contact between the semicrystals, sudden mechanical loads and shear stresses develop. Starting from the surface and extending successively to the interior of semicrystals, local shear stresses mediated by force chains determine an extensive rearrangement of atomic positions. These induce interfacial mixing processes that finally result in the formation of a structurally disordered region at the interface. Its thickness increases with time according to a power law

similar to the one characteristic of thermal diffusion. In this case, however, atomic displacements are due to shear events. Thermal rearrangement processes becomes important after the removal of mechanical forces, when a relatively fast relaxation takes place determining the disappearance of force chains.

Far from being exhaustive, the numerical findings point out the important role played by the shear-induced displacements of atomic species in the formation of a disordered interface. The numerical evidences here discussed, restricted to the early stages of the impact event, should be intended as only indicative. Further studies must be carried out to gain adequate insight into the mechanistic features of the shear-induced transformations.

ACKNOWLEDGMENTS

Financial support has been provided by the University of Sassari and the University of Cagliari. A. Ermini, ExtraInformatica s.r.l., is gratefully acknowledged for the technical support.

*Electronic address: delogu@dicm.unica.it

[1] *Physical Metallurgy*, 4th revised and enhanced edition, edited by R. W. Cahn, P. Haasen (Elsevier Science, BV, 1996).
[2] K. E. Easterling and D. A. Porter, *Phase Transformations in Metals and Alloys*, 2nd edition (Chapman & Hall, London, UK, 1992).
[3] C. Kittel, *Introduction to Solid State Physics*, 7th edition (Wiley, New York, 1996).
[4] G. Heinicke, *Tribochemistry* (Akademie-Verlag, Berlin, 1984).
[5] P. Yu. Butyagin, Sov. Sci. Rev. **14**, 1 (1989).
[6] C. Suryanarayana, Prog. Mater. Sci. **46**, 1 (2001).
[7] B. B. Khina and F. H. Froes, J. Met. **48**, 36 (1996).
[8] T. H. Courtney, Mater. Trans., JIM **36**, 110 (1995).
[9] P. Bellon and R. S. Averback, Phys. Rev. Lett. **74**, 1819 (1995).
[10] J. E. Hammerberg, B. L. Holian, J. Roder, A. R. Bishop, and S. J. Zhou, Physica D **123**, 330 (1998).
[11] R. G. Hoagland and M. I. Baskes, Scr. Mater. **39**, 417 (1998).
[12] V. Bulatov, F. F. Abraham, L. Kubin, B. Devincre, and S. Yip, Nature (London) **391**, 669 (1998).
[13] I. A. Ovid'ko and A. B. Reizis, J. Phys. D **32**, 2833 (1999).
[14] X. Y. Fu, M. L. Falk, and D. A. Rigney, Friction Wear **250**, 420 (2001).
[15] M. F. Horstemeyer, M. I. Baskes, and S. J. Plimpton, Acta Mater. **49**, 4363 (2001).
[16] K. Kadau, T. C. Germann, P. S. Lomdahl, and B. L. Holian, Science **296**, 1681 (2002).
[17] A. C. Lund and C. A. Schuh, Appl. Phys. Lett. **82**, 2017 (2003).
[18] V. I. Levitas, Phys. Rev. B **70**, 184118 (2004).
[19] F. Delogu and G. Cocco, Phys. Rev. B **71**, 144108 (2005).
[20] F. Delogu and G. Cocco, Phys. Rev. B **72**, 014124 (2005).
[21] W. L. Johnson, Prog. Mater. Sci. **30**, 81 (1986).
[22] W. J. Meng, C. W. Nieh, and W. L. Johnson, Appl. Phys. Lett. **51**, 1693 (1987).
[23] U. Gosele and K. N. Tu, J. Appl. Phys. **66**, 2619 (1989).
[24] R. J. Highmore, Philos. Mag. B **62**, 455 (1990).
[25] L. Greer, Philos. Mag. B **61**, 525 (1990).
[26] R. Yavari and P. J. Desrè, Mater. Sci. Forum **88–90**, 43 (1992).
[27] C. Massobrio, V. Pontikis, and G. Martin, Phys. Rev. B **41**, 10486 (1990).
[28] V. Rosato, M. Guillope, and B. Legrand, Philos. Mag. A **59**, 321 (1989).
[29] F. Ducastelle, J. Phys. (Paris) **31**, 1055 (1970).
[30] P. Mura, P. Demontis, G. B. Suffritti, V. Rosato, and M. Vittori-Antisari, Phys. Rev. B **50**, 2850 (1994).
[31] M. P. Allen and D. Tildesley, *Computer Simulation of Liquids* (Clarendon Press, Oxford, U.K., 1987).
[32] S. Nosè, J. Chem. Phys. **81**, 511 (1984).
[33] M. Parrinello and A. Rahman, J. Appl. Phys. **52**, 7182 (1981).
[34] F. Delogu, L. Schiffini, and G. Cocco, Philos. Mag. A **81**, 1917 (2000).
[35] L. A. Braunstein, S. V. Buldyrev, S. Havlin, and H. E. Stanley, Phys. Rev. E **65**, 056128 (2002).
[36] J. Casas-Vazquez and D. Jou, Rep. Prog. Phys. **66**, 1937 (2003).
[37] L. Gomez, A. Dobry, C. Geuting, H. T. Diep, and L. Burakovsky, Phys. Rev. Lett. **90**, 095701 (2003).